JOURNAL OF NANO- AND ELECTRONIC PHYSICS
Vol. **18** No 2, 02004(11pp) (2026)

ЖУРНАЛ НАНО- ТА ЕЛЕКТРОННОЇ ФІЗИКИ
Том **18** № 2, 02004(11cc) (2026)

OPEN ACCESS

REGULAR ARTICLE

Simulation of Wave Propagation in a Kerr-Type Nonlinear Metamaterial Cylindrical Wave-Guide by Auxiliary Differential Equation Finite Difference Time Domain Method

A. Yalçınkaya[1,*], A. Çetin[2†]

[1] *Eskişehir Osmangazi University, Graduate School of Natural and Applied Sciences, Eskişehir, Turkiye*
[2] *Eskişehir Osmangazi University, Faculty of Science, Meşelik Kampüsü, Eskişehir, Turkiye*

(Received 03 February 2026; revised manuscript received 18 April 2026; published online 29 April 2026)

Propagation of electromagnetic waves and mode formation in a cylindrical waveguide with double negative metamaterial core having Kerr type nonlinearity is investigated in this study using auxiliary differential equation finite difference time domain method. Propagation in one-dimensional, two-dimensional, and three-dimensional configurations are explored, and the interaction of properties relevant to dispersion, non-linearity and cylindrical structure is highlighted emphasizing its influence on mode behavior. Discretized equations presented in the paper are different from all the equations presented in previous finite difference time domain-based research and relevant literature. The novel application used in this work for investigating wave dynamics in a cylindrical core of completely double negative metamaterial showed new findings. Backward wave propagation and self-focusing nonlinear modes are observed due to double negative proper-ties and Kerr effect as expected. The results are expected to enhance research on nonlinear fiberoptics and attract attention to metamaterials and how the effect of losses is observed in metamaterial waveguides.

Keywords: Metamaterial, Cylindrical waveguide, Kerr nonlinearity, Finite difference time domain, Auxiliary differential equation.

DOI: 10.21272/jnep.18(2).02004 PACS numbers: 42.25.Bs, 42.65.Wi, 42.81.Qb

1. INTRODUCTION

Metamaterials (MTMs) with simultaneously negative permittivity (ε) and permeability (μ), which were introduced by Veselago [1] and experimentally verified by Shelby et al. [2], are known as double negative (DNG) or left-handed materials (LHMs). They are spreadingly drawing attention due to their extraordinary features not found in conventional materials. As they have artificial periodic structures making it possible to modify permittivity and permeability, dispersion of waves can be controlled, and many novel applications are possible. These materials exhibit unusual electromagnetic properties such as negative refraction, subwavelength focusing, and backward wave propagation [3]. They support unconventional electromagnetic modes.

Waveguides with cylindrical structure and MTMs as well as other nonlinear medium drew interest as various properties of the MTMS not available in right-handed materials (RHMs) present potential for new applications, and significant number of research has been done on cylindrical waveguides with especially MTM claddings [4-7], or partially filled MTM core [8, 9]. Cylindrical waveguides with DNG cores have interesting configuration due to their potential to support novel unconventional electromagnetic modes, below-cutoff propagation and backward waves being some of the outcomes [4, 10, 11]. Some studies examining linear DNG waveguides have been presented [10], but studies of them where the DNG core has Kerr nonlinearity which introduces intensity dependent permittivity is still underexplored. From previous studies, nonlinear responses can result in self-focusing and power dependent mode properties or can lead to soliton formation [12].

The essential numerical method used in this study is the Finite Difference Time Domain (FDTD) approach, a method based on Yee lattice and algorithm [13] and used for wave propagation in linear medium in cartesian coordinates [14, 15], nonlinear medium in Cartesian coordinates [16-18] as well as cylindrical coordinates [19, 20], and for solutions of various structures.

For simulation of the cylindrical waveguide, we employ the auxiliary differential equation finite difference time domain method (ADE-FDTD), which is highly effective for dispersive and nonlinear media [18, 21, 22], not forgetting the attention to coordinate singularities [3, 19, 21]. The Kerr type nonlinear waveguide core is modelled using Drude dispersion for permittivity and Lorentz dispersion for permeability, a model proven to be convenient for DNG metamaterials [19, 24]. For a comprehensive presentation of the waveguide behaviour, one- two- and three-dimensional (1D, 2D, 3D) simulations are implemented. All the graphics or figures are outputs of the simulation carried out using Python.

* Correspondence e-mail: 501320201001@ogrenci.ogu.edu.tr
† acetin@ogu.edu.tr

Cite this article as: A. Yalçınkaya et al., *J. Nano- Electron. Phys.* 18 No 2, 02004 (2026) https://doi.org/10.21272/jnep.18(2).02004

2. THEORY AND MATHEMATICAL FORMULATION

It can be shown in a cylindrical waveguide with wave propagation in z direction that for linear, nondispersive, and isotropic case, the longitudinal electric field component changes only with the radial coordinate r due to its harmonic behaviour and due to circular symmetry of the cylindrical structure. The field modes are TE modes depending on the radial parameter.

A cylindrical waveguide with a DNG negative-index metamaterial core with radius R, and with the longitudinal position on z axis placed in the centre of that core, i.e. on the centreline of the cylinder is shown in Fig. 1. It should not be forgotten that the waveguide is assumed to be infinite in y and z directions. The research is restricted to the linear conventional materials for cladding, and perfect electric conductor (PEC) for simulation case studies in this paper.

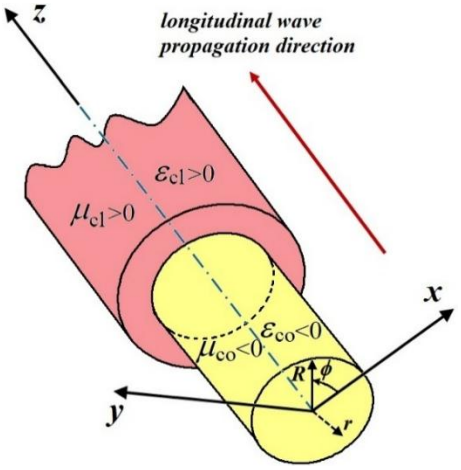

Fig. 1 – Cylindrical waveguide with metamaterial core

Regarding the parameters, R is the core radius, $b = R - R_{cl}$ is the cladding width, ε_{co}, μ_{co} and ε_{cl}, μ_{cl} are respectively the permittivity and permeability of the core and cladding.

2.1 Dispersion Models for Metamaterials

As a dispersive DNG metamaterial is considered for the core, both permittivity and permeability are frequency dependent and they are modelled using Drude and Lorentz models respectively, expressed as

$$\varepsilon(\omega)=\varepsilon_0\left(1-\frac{\omega_p^2}{\omega(\omega+i\gamma_e)}\right), \tag{1}$$

$$\mu(\omega)=\mu_0\left(1+\frac{\omega_m^2}{\omega_0^2-\omega^2-i\omega\gamma_m}\right) \tag{2}$$

where ω_p is the electric plasma frequency, ω_m the magnetic plasma frequency, γ_e the electric damping coefficient, γ_m the magnetic damping coefficient, and ω_0 is the magnetic resonance frequency.

Reel and imaginary parts of the permittivity and permeability for the related Drude and Lorentz models are shown in Fig. 2.

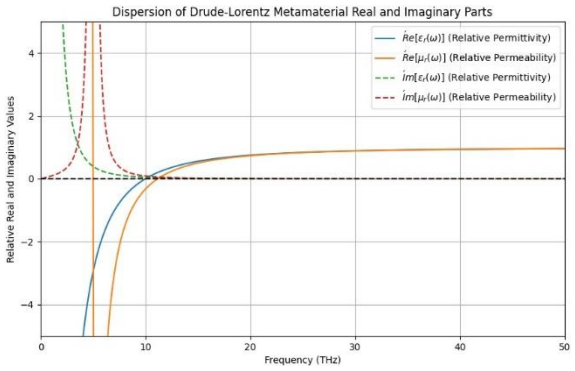

Fig. 2 – Drude-Lorentz model dispersion: real and imaginary parts of permittivity and permeability

The core is double negative so that both the permittivity and permeability are negative in this region, and the negative value of the refractive index is chosen as the square root of $\varepsilon_{co}\mu_{co}$ can be either positive or negative. Imaginary part of the permeability is mainly responsible for the highest part of the losses.

2.2 Auxiliary Differential Equation Finite Difference Time Domain (ADE-FDTD)

Conventional FDTD method in cylindrical coordinates has established itself to be an effective method for simulation of nondispersive natural materials [26]. In cases where dispersive nonlinear materials are in question, however, the ADE-FDTD shows itself as an easy and reliable method for treatment of wave propagation in such media [17].

This method introduces auxiliary differential equations for polarization as well as magnetization where applicable to handle dispersive and nonlinear materials [21].

With the dispersive behaviour of permittivity and permeability, magnetic flux density and electric displacement are $\boldsymbol{B}=\mu(\omega)\boldsymbol{H}$ and $\boldsymbol{D}=\varepsilon(\omega)\boldsymbol{E}$ respectively. Considering the contributions of the Drude electric current $\boldsymbol{J}$, polarization $\boldsymbol{P}=\boldsymbol{P}_L+\boldsymbol{P}_{NL}$ and magnetization $\boldsymbol{M}$, electric displacement and magnetic flux density are respectively expressed as $\boldsymbol{D}=\varepsilon(\omega)\boldsymbol{E}+\boldsymbol{P}$ and $\boldsymbol{B}=\mu(\omega)\boldsymbol{H}+\boldsymbol{M}$ so that Maxwell Curl Equation describing Faraday law becomes

$$\nabla\times\boldsymbol{E}=-\mu\frac{\partial\boldsymbol{H}}{\partial t}-\frac{\partial\boldsymbol{M}}{\partial t} \tag{3}$$

and Maxwell Curl Equation describing Ampere law becomes

$$\nabla\times\boldsymbol{H}=\varepsilon\frac{\partial\boldsymbol{E}}{\partial t}+\boldsymbol{J}+\frac{\partial\boldsymbol{P}_{NL}}{\partial t}+\frac{\partial\boldsymbol{P}_L}{\partial t} \tag{4}$$

where the linear part of polarization is related to the dispersion model, and the nonlinear part for a metamaterial with Kerr-type nonlinearity can be written as

$$\boldsymbol{P}_{NL}=\varepsilon_0\chi^{(3)}\left|\boldsymbol{E}^2\right|\boldsymbol{E} \tag{5}$$

With $\chi^{(3)}$ being the 3rd order susceptibility as a factor of the Kerr nonlinearity [12].

Using Drude and Lorentz dispersive models for permittivity and permeability respectively in the equations for magnetic flux and electric displacement, and taking inverse Fourier transform of them, we obtain the auxiliary differential equations for polarization and magnetization as

$$\frac{\partial^2 \boldsymbol{P}}{\partial t^2} + \gamma_e \frac{\partial \boldsymbol{P}}{\partial t} = \varepsilon_0 \omega_p^2 \boldsymbol{E} \,, \tag{6}$$

$$\frac{\partial^2 \boldsymbol{M}}{\partial t^2} + \gamma_m \frac{\partial \boldsymbol{M}}{\partial t} + \omega_0^2 \boldsymbol{M} = \mu_0 \omega_m^2 \boldsymbol{H} \tag{7}$$

These equations are concurrently solved with the Maxwell equations for implementation of the simulation.

Eqs. (3) and (4) are expressed in cylindrical coordinates for their field components in most general case as

$$\frac{\partial H_\varphi}{\partial t} = -\frac{1}{\mu}\left(\frac{\partial E_r}{\partial z} - \frac{\partial E_z}{\partial r}\right) - \frac{1}{\mu}\frac{\partial M_\varphi}{\partial t} \,, \tag{8}$$

$$\frac{\partial H_r}{\partial t} = -\frac{1}{\mu}\left(\frac{1}{r}\frac{\partial E_z}{\partial \varphi} - \frac{\partial E_\varphi}{\partial z}\right) - \frac{1}{\mu}\frac{\partial M_r}{\partial t} \,, \tag{9}$$

$$\frac{\partial H_z}{\partial t} = -\frac{1}{\mu}\left(\frac{1}{r}\frac{\partial (rE_\varphi)}{\partial r} - \frac{1}{r}\frac{\partial E_r}{\partial \varphi}\right) - \frac{1}{\mu}\frac{\partial M_z}{\partial t} \,, \tag{10}$$

$$\frac{\partial E_\varphi}{\partial t} = \frac{1}{\varepsilon}\left(\frac{\partial H_r}{\partial z} - \frac{\partial H_z}{\partial r}\right) - \frac{1}{\varepsilon}J_\varphi - \frac{1}{\varepsilon}\left(\frac{\partial P_{L,\varphi}}{\partial t} + \frac{\partial P_{NL,\varphi}}{\partial t}\right), \tag{11}$$

$$\frac{\partial E_r}{\partial t} = \frac{1}{\varepsilon}\left(\frac{1}{r}\frac{\partial H_z}{\partial \varphi} - \frac{\partial H_\varphi}{\partial z}\right) - \frac{1}{\varepsilon}J_r - \frac{1}{\varepsilon}\left(\frac{\partial P_{L,r}}{\partial t} + \frac{\partial P_{NL,r}}{\partial t}\right), \tag{12}$$

$$\frac{\partial E_z}{\partial t} = \frac{1}{\varepsilon}\left(\frac{1}{r}\frac{\partial (rH_\varphi)}{\partial r} - \frac{1}{r}\frac{\partial H_r}{\partial \varphi}\right) - \frac{1}{\varepsilon}J_z - \frac{1}{\varepsilon}\left(\frac{\partial P_{L,z}}{\partial t} + \frac{\partial P_{NL,z}}{\partial t}\right) \tag{13}$$

In special cases, as in the simulation example in Sections 3 and 4, assuming $\partial(\partial\varphi)^{-1} = 0$ due to azimuthal symmetry and remembering that TM mode configuration is considered, so some of the fields become $E_r = 0$, $E_\varphi = 0$, and $H_z = 0$. There will be no longitudinal variation in 1D radial propagation so that $\partial(\partial z)^{-1}$ is going to vanish and $H_r = 0$. This special case in simulation is actually a type of analysis of mode cutoff behaviour or nonlinear self-focusing in the transverse plane and represent time evolution of the mode shape without considering propagation along the z direction. It gives insight to understand radial confinement, mode formation, and nonlinear transverse effects.

To solve Eqs. (8) to (13) using FDTD, discretized form of them is obtained using the Yee algorithm [14] but for cylindrical coordinates r, φ, and z [2]. Central difference approach is used for the finite differences. In deriving the discretised equations, we use the leapfrog approach which suggests for time steps integer n for E and half-integer $n + 1/2$ for H. The resulting equations after discretizing and arranging are for magnetic and electric fields respectively.

$$H_\varphi^{n+1/2}[i,k] = H_\varphi^{n-1/2}[i,k] - \frac{\Delta t}{\mu} C1_{r,z}^n - \frac{1}{\mu} C2_\varphi^n \,, \tag{14}$$

$$H_r^{n+1/2}[i+1/2,k+1/2] = H_r^{n-1/2}[i+1/2,k+1/2] - \frac{\Delta t}{\mu} C3_\varphi^n - \frac{1}{\mu} C4_r^n \,, \tag{15}$$

$$H_z^{n+1/2}[i,k+1/2] = H_z^{n-1/2}[i,k+1/2] - \frac{\Delta t}{\mu} C5_{\varphi,r}^n - \frac{1}{\mu} C6_z^n \,, \tag{16}$$

$$E_r^{n+1}[i,k+1/2] = E_r^n[i,k+1/2] - \frac{\Delta t}{\varepsilon}(C7_\varphi^n + J_r^{n+1/2}[i,k]) - \frac{1}{\varepsilon} C8_r^n \,, \tag{17}$$

$$E_\varphi^{n+1}[i+1/2,k] = E_\varphi^n[i+1/2,k] - \frac{\Delta t}{\varepsilon}(C9_{r,z}^n + J_\varphi^{n+1/2}[i,k]) - \frac{1}{\varepsilon} C10_\varphi^n \,, \tag{18}$$

$$E_z^{n+1}[i+1/2,k] = E_z^n[i+1/2,k] - \frac{\Delta t}{\varepsilon}(G1_\varphi^n + J_z^{n+1/2}[i,k]) - \frac{1}{\varepsilon} G2_z^n \,, \tag{19}$$

where the details of the implicit expressions C1 to G2, and all similar terms C2 to C10, G3 to G10, F1 to F9 and A1 to A6 are given in the Appendix.

For the case of TE mode configuration, assuming $\partial(\partial\varphi)^{-1} = 0$ due to azimuthal symmetry so that at the end $E_z = 0$, $H_\varphi = 0$, and $H_r = 0$. For this special case, Eqs. (8) to (13) for the available field components become in cylindrical coordinates as

$$\frac{1}{r}\frac{\partial (rE_\varphi)}{\partial r} = -\mu \frac{\partial H_z}{\partial t} \,, \tag{20}$$

$$\frac{\partial H_z}{\partial r} = \varepsilon \frac{\partial E_\varphi}{\partial t} \,, \tag{21}$$

$$-\frac{\partial H_z}{\partial z} = \varepsilon \frac{\partial E_r}{\partial t} \tag{22}$$

The discretized equations for ADE-FDTD solution of Eq. (20), Eq. (21), and Eq. (22) for magnetic and electric field after arranging will be

$$H_z^{n+1/2}[i,k] = H_z^{n-1/2}[i,k] - \frac{\Delta t}{\mu[i,k] r[i] \Delta r} G3_\varphi^n \,, \tag{23}$$

$$E_\varphi^{n+1}[i+1/2,k] = E_\varphi^n[i+1/2,k] - \frac{\Delta t}{\varepsilon[i+1/2,k]\Delta r} G4_z^n \tag{24}$$

$$E_r^{n+1}[i,k+1/2] = E_r^n[i,k+1/2] - \frac{\Delta t}{\varepsilon[i,k+1/2]\Delta z} G5_z^n \tag{25}$$

3. IMPLEMENTATION PARAMETERS AND ASSUMPTIONS

Equations for simulation of the propagation for TM and TE configurations are implemented with assumptions regarding the parameters of the dispersion models, geometric dimensions of the waveguide, parameters of the FDTD method, coefficients and other relevant information.

Simulation is carried out employing ADE-FDTD method for three configurations of spatial propagation where suitable assumptions are made for both simplicities, as well as the features of the problem or model.

3.1 One-Dimensional Simulation (1D)

In one-dimensional simulation, field components are changing only with the radial coordinate. A linear and a nonlinear case are simulated. Additionally, a simulation for 1D propagation in the longitudinal direction is also given.

A linear, nondispersive and lossy material for the sake of comparison opportunity is simulated for TM configuration with application of a Gaussian beam as a source simulation having a profile

$$E_{sz} = \frac{1-\cos(\frac{2\pi t}{w})}{2} e^{-((t-\frac{w}{2})/6)^2} \tag{26}$$

with pulse width $w = 30$. The source is placed on 1/3rd of the radial position. The electric-field envelope is Gaussian both in space (transverse beam width) and time (pulse duration). This Gaussian profile ensures smooth excitation, smooth onset and decay reducing numerical artifacts, and the beam is well-confined spatially, representing a realistic laser-like excitation. The time modulation makes it a finite pulse.

Discretized equations for simulation are as below for radial confinement, and Fig. 3 gives snapshots of the field profiles for radial change

$$H_\varphi^{n+1}[i] = H_\varphi^n[i] - \frac{\Delta t}{\mu[i]\Delta r}\left(E_z^n[i+1] - E_z^n[i]\right), \tag{27}$$

$$E_z^{n+1}[i] = E_z^n[i] - \frac{\Delta t}{\varepsilon[i]\Delta r}\left(H_\varphi^n[i] - H_\varphi^n[i-1]\right) \tag{28}$$

If we consider longitudinal dynamics, discretized equations will be as below, and snapshots of longitudinal propagation are also given in Fig. 3

$$H_\varphi^{n+1/2}[i] = H_\varphi^{n-1/2}[i] - \frac{\Delta t}{\mu_0\Delta z}\left(E_z^n[i+1] - E_z^n[i]\right), \tag{29}$$

$$E_z^{n+1}[i] = E_z^n[i] - \frac{\Delta t}{\varepsilon[i]\Delta z}\left(H_\varphi^{n+1/2}[i] - H_\varphi^{n-1/2}[i-1]\right) \tag{30}$$

where $\Delta t \le \Delta z/c$ with $\Delta t = \Delta z/2c$ used in the simulation c being the speed of light, and $\mu = \mu_0$ taken for simplicity.

The $E_z{}^n$ in Eqs. (27) and (29) may be seen problematic in terms of physical consistency and numerical stability. This is true in general and especially when nonlinearity is strong. In this study, susceptibility is very small, i.e. $\chi^{(3)} = 10^{-20}$ m²V^{-2} which means that Kerr nonlinearity is very weak in this case. So, the possible stability problem is reduced although $E_z{}^{n+1}$ is not applied and cubic equation iterations are avoided with the explicit scheme used.

Similarly, a nonlinear, dispersive and lossy material is simulated for TM configuration with again application of a Gaussian beam as a source given as

$$E_{sz} = e^{-((t-\frac{w}{2})/5)^2} \tag{31}$$

with pulse width $w = 40$. The source is placed on the half of radial position.

ADE-FDTD equations discretized for simulation of the nonlinear dispersive MTM are given in Eq. (32) to Eq. (35). As easily noticed, the solution of equations for magnetic field and electric field are to be solved concurrently with the equations for magnetization and polarization. In the numerical examples in simulation of 1D propagation, ε_0 is used for simplicity.

$$H_\varphi^{n+1}[i] = H_\varphi^n[i] - \frac{\Delta t}{\mu_0\Delta r} G6_{z,\varphi}^n, \tag{32}$$

$$E_z^{n+1}[i] = E_z^n[i] - \frac{\Delta t}{\varepsilon[i]} G7_{\varphi,z}^n, \tag{33}$$

$$M_\varphi^{n+1}[i] = M_\varphi^n[i] - \Delta t G8_\varphi^n, \tag{34}$$

$$P_z^{n+1}[i] = P_z^n[i] + \Delta t(\varepsilon_0\omega_p^2 E_z[i] - \gamma_e P_z[i]) \tag{35}$$

3.2 Two-Dimensional Simulation (2D)

In two-dimensional simulations, field components are dependent on the radial and longitudinal coordinates. Again, the simulation is carried out for a linear and for a nonlinear case to have a comparative insight.

A linear nondispersive material close to air parameter conditions, i.e. $\varepsilon = \varepsilon_0$, and $\mu = \mu_0$, simulated for TM configuration so that $E_r = H_r = 0$. Zero Dirichlet boundary conditions applied as r^{-1} terms and corrections are ignored for handling singularities. Azimuthal symmetry is assumed. A Gaussian pulse used for excitation, namely

$$E_{sz}(r_0, z_0, t) = \sin(2\pi f_s t) e^{-\frac{1}{2}(\frac{t-w}{\sigma})^2} \tag{36}$$

is applied where r_0 – centre of radial range, z_0 – one fourth of longitudinal range, w – pulse width, $\sigma - w\Delta t$, f_s – source frequency = 10 GHz, Δt – time step value, n –time step index, $E_{zs}(r,z,t)$ is the source electric field component at point (r,z,t), and $t = n\Delta t$ is current time. This source is time modulated with sinusoidal carrier and is Gaussian-enveloped, exciting a band of frequencies around f_s. It is placed at the center radially and at one-fourth of the longitudinal domain. It resembles initially the linear Gaussian shape, but with time, deformation begins due to nonlinear response. As the nonlinear Kerr-type media cause intensity-dependent refractive index variation, also the source region shows deviation from perfect Gaussian with the evolution of time.

Eqs. (20) to (22) are valid also for the TM mode in linear 2D with the only difference that ε_0 and μ_0 is chosen respectively for permittivity and permeability for simplicity due to nondispersive nature of the linear case considered. Corresponding discretized equations after some arrangements come out to be

$$H_\varphi^{n+1/2}[i+1/2,k] = H_\varphi^{n-1/2}[i+1/2,k] + \frac{\Delta t}{\mu_0} G9_z^n, \tag{37}$$

$$H_r^{n+1/2}[i,k+1/2] = H_r^{n-1/2}[i,k+1/2] + \frac{\Delta t}{\mu_0} G10_z^n, \tag{38}$$

$$E_z^{n+1}[i,k] = E_z^{n+1}[i,k] + \frac{\Delta t}{\varepsilon_0} F1_{r,z,\varphi}^n \quad , \tag{39}$$

where $\Delta z = \Delta r = 1$ mm, $\Delta t = 0.99c^{-1}((\Delta r)^{-2} + (\Delta z)^{-2})^{-1/2}$ also known as Courant–Friedrichs–Lewy (CFL) condition, with grid sizes in r and z as 100 and 200 respectively.

For the nonlinear material core, the Gaussian pulse excited is the same as used in the linear case. For both, grid size: 100×200 cells, spatial steps being $\Delta r = \Delta z = 1$ mm, source is a modulation of a 10 GHz Gaussian pulse.

Governing equations for TM configuration are as below for Kerr-type nonlinear double negative lossy metamaterials with Drude model permittivity dispersion and Lorentz model permeability dispersion

$$\frac{\partial H_\varphi}{\partial t} = -\frac{1}{\mu}\left(\frac{\partial E_z}{\partial r} - \frac{\partial E_r}{\partial z}\right) - \frac{1}{\mu_0}\frac{\partial M_\varphi}{\partial t} \quad , \tag{40}$$

$$\frac{\partial E_r}{\partial t} = \frac{1}{\varepsilon_0 \varepsilon_\infty}\left(\frac{1}{r}\frac{\partial (rH_\varphi)}{\partial z} - \frac{\partial P_{L,r}}{\partial t} - \frac{\partial P_{NL,r}}{\partial t} - -J_{D,r}\right), \tag{41}$$

$$\frac{\partial E_z}{\partial t} = \frac{1}{\varepsilon_0 \varepsilon_\infty}\left(-\frac{\partial H_\varphi}{\partial r} - \frac{\partial P_{NL,z}}{\partial t} - \frac{\partial P_{L,z}}{\partial t} - J_{D,z}\right) \tag{42}$$

where M is the magnetic polarization or magnetization component due to Lorentz resonance, with the same direction as the magnetic field. PML absorbing layer boundary conditions are assumed. $J_{D,r}$ and $J_{D,z}$ are the radial and longitudinal components of the Drude current respectively. Drude current and $P_{NL,z}$, $P_{L,z}$, $P_{NL,r}$ and $P_{L,r}$ which are respectively the longitudinal and radial components of the electric polarization and Lorentz polarization come from the Drude dispersion. Nonlinear terms of polarization are distinguished with their subscript NL.

Since we deal with TM modes, discretized update equations for the fields in our simulation are obtained as not to forget, of course, that at $r = 0$, the first term ($F5$, i.e. term involving H_φ, see Appendix) in Eq. (45) is multiplied by 2 due to symmetry.

$$H_\varphi^{n+1/2}[i,k] = H_\varphi^{n-1/2}[i,k] - \frac{\Delta t}{\mu_0 \mu_\infty} F2_{r,z}^n - \frac{\Delta t}{\mu_0} F3_\varphi^n \quad , \tag{43}$$

$$E_r^{n+1}[i,k] = E_r^n[i,k] + \frac{\Delta t}{\varepsilon_0 \varepsilon_\infty}(F4_{r,\varphi}^n - F5_r^n - J_{D,r}^{n+1}[i,k]) \quad , \tag{44}$$

$$E_z^{n+1}[i,k] = E_z^n[i,k] + \frac{\Delta t}{\varepsilon_0 \varepsilon_\infty}(F6_{r,\varphi}^n - F7_z^n - J_{D,z}^{n+1}[i,k]) \tag{45}$$

In our relevant simulation, we take high frequency permittivity and permeability as $\varepsilon_\infty = 1.5$, and $\mu_\infty = 1.0$ respectively.

3.3 Three-Dimensional Simulation (3D)

In three-dimensional simulations, field components are dependent on all the cylindrical coordinates and may show various unusual behaviour when the core material is a DNG metamaterial of the previously mentioned type.

Simulations of various linear non-dispersive cylindrical wave propagation have been investigated in literature. We carry out the simulation in this paper for nonlinear dispersive cases using the Kerr-type material and observe the results for different values or ranges.

The excitation applied in the simulation of the nonlinear axisymmetric propagation is a hard excitation, an oscillating Gaussian beam expressed as

$$E_{zs}(r, z_0, t) = E_0 A(r) \sin(\omega_c t) e^{-\frac{(t-t_0)^2}{w_t}} \tag{46}$$

where $\omega_c = 210^{10}$ s^{-1} is carrier wave frequency, $A(r)$ is the radial mode profile, $w_t = 1{,}44 \times 10^{-22}$ s is the pulse width, $t_0 = 2 \times 10^{-11}$ s is the time at 1/6th of the z_{max} pulse centre, z_0 is the fixed source excitation plane, and $E_0 = 2 \times 10^5$ Vm^{-1} is the amplitude. This beam is a physically reasonable excitation. It is numerically stable, without artificial oscillations, with a good alignment and remaining symmetric.

If we consider a linear and nondispersive core material, with some simplifications such as taking respectively μ_0 and ε_0 for permeability and permittivity, the field equations obtained for the TM mode will be considering $\partial(\partial\varphi)^{-1} = 0$ due to axial symmetry which, of course, leads the field to vary only with one spatial variable r together with t.

$$\frac{\partial H_\varphi}{\partial t} = \frac{1}{\mu_0}\frac{\partial E_z}{\partial r} \quad , \tag{47}$$

$$\frac{\partial H_r}{\partial t} = \frac{1}{\mu_0}\frac{\partial E_z}{\partial z} \quad , \tag{48}$$

$$\frac{\partial E_z}{\partial t} = \frac{1}{\varepsilon_0}\left(\frac{1}{r}\frac{\partial (rH_\varphi)}{\partial z} + \frac{\partial H_r}{\partial z}\right) \tag{49}$$

Simple Dirichlet condition is assumed for boundary conditions. So, after some arrangements, the corresponding discrete update equations H_φ and E_z come out as

$$H_\varphi^{n+1/2}[i+1/2,k] = H_\varphi^{n-1/2}[i+1/2,k] - \frac{\Delta t}{\mu_0} F8_z^n \quad , \tag{50}$$

$$H_r^{n+1/2}[i,k+1/2] = H_r^{n-1/2}[i,k+1/2] - \frac{\Delta t}{\mu_0} F9_z^n \quad , \tag{51}$$

$$E_z^{n+1}[i,k] = E_z^{n+1}[i,k] + \frac{\Delta t}{\varepsilon_0} A1_{z,r,\varphi}^n \tag{52}$$

with $\Delta z = \Delta r = 1$ mm, and $\Delta t \le 0.35c^{-1}((\Delta r)^{-2} + (\Delta z)^{-2})^{-1/2}$ a CFL condition for this special case, with grid sizes in r and z as 80 and 200 respectively.

In case of nonlinear dispersive core, after some assumptions and selections by taking in simulation one-component form (one electric and one magnetic field) to simplify the model for cylindrical waveguide with metamaterial core having Drude permittivity, Lorentz permeability, and Kerr-type nonlinearity, and a perfect electric conductor cladding, governing 3D field equations are yielded as

$$\frac{\partial H_\varphi}{\partial t} = \frac{1}{\mu(\omega)}\left(\frac{\partial E_z}{\partial r} - \frac{\partial M_\varphi}{\partial t}\right), \tag{53}$$

$$\frac{\partial E_z}{\partial t} = \frac{1}{\varepsilon(\omega, \boldsymbol{E})}\left(\frac{\partial H_\varphi}{\partial r} + \frac{H_\varphi}{r} - \frac{\partial P_z}{\partial t} - P_{NL,z}\right), \tag{54}$$

For simplicity, we choose in our simulation example ε_0 for permittivity and μ_0 for permeability which would limit the field to certain frequencies but acceptable. With this assumption, discretized update equations for the magnetic and electric fields given in Eq. (53) and Eq. (54) are then

$$H_\varphi^{n+1}[i+1/2,k] = H_\varphi^n[i+1/2,k] - \frac{\Delta t}{\mu_0}(A2_{r,z}^n + A3_\varphi^n), \tag{55}$$

$$E_z^{n+1}[i,k] = E_z^n[i,k] + \frac{\Delta t}{\varepsilon_0}(A4_{r,\varphi}^n - A5_z^n + A6_{r,\varphi,z}^n) \tag{56}$$

4. RESULTS AND DISCUSSIONS

The 1D simulation of a linear MTM, snapshots of which are given in Fig. 6 show the electric and magnetic field behaviours in the DNG region. Increasing time steps demonstrate the homogeneity of the propagation. For comparison, the cladding is also shown on the graphics to be able to comprehend the difference between the two regions.

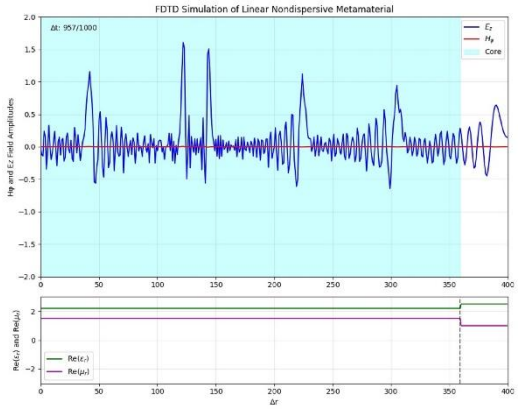

a

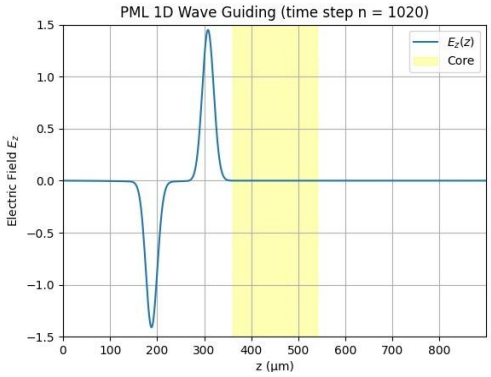

b

Fig. 3 – Snapshots from the 1D simulation of the wave propagation: a) linear nondispersive material at $t = 957\Delta t$ showing the case of changes only in the radial direction, c) linear nondispersive material at $t = 1020\Delta t$ showing the propagation in the longitudinal direction

For simulation, radius of the core is taken as 10 mm, 200 points selected as resolution, time step is subject to stability condition and expressed as $\Delta t \le 0.99\Delta r(2c)^{-1}$ with c as the speed of light, 1000-time steps are applied, 400 radial points are used. Material parameters are $\varepsilon_{co} = -2.2 + 0.1j$, $\mu_{co} = -1.5 + 0.1j$ and $\varepsilon_{cl} = 2.5$, $\mu_{cl} = 1.0$. First order absorbing boundary conditions (ABCs) applied. The model is approximated neglecting r^{-1} terms to avoid singularities.

In simulation for the nonlinear case, radius of the core and number of points as resolution are the same as in the linear case. Time step is subject to stability condition and expressed this time as $\Delta t \le 0.5(\Delta r)c^{-1}$, 500-time steps are applied, and 1000 radial points are used. Material parameters are Drude model dispersion for permittivity, and Lorentz model dispersion for the permeability of the core. Permittivity and permeability of the cladding are the same values used for linear case. Simple 1st order ABCs applied. Kerr type nonlinearity with extra term $3\chi^{(3)}E^2E$. Parameters for dispersion models are: Plasma frequency $\omega_p = 4\pi 10^{10}$ s^{-1}, damping coefficient $\gamma_e = \pi 10^{12}$ s^{-1}, resonance frequency $\omega_0 = 5\pi 10^{10}$ s^{-1}, magnetic plasma frequency $\omega_m = 4\pi 10^{11}$ s^{-1}, magnetic damping $\gamma_m = 4\pi 10^{11}$ s^{-1}, and $\chi^{(3)} = 10^{-20}$ m^{2}V^{-2}.

When the core material is DNG with Key type nonlinearity, having Drude-Lorentz model dispersion respectively, behaviour of the field profiles changes., and inhomogeneous variations with time characterize both forward modes as well as field profiles with phase reversals as shown in Fig. 4. To get a clear visualization, snapshots for the field strength are given with closer views of the field strength axis for different amplified absolute values of the electric and magnetic fields.

Radial dependence can be correlated with standing waves and there is no outward energy propagation radially. Radial fields oscillate.

In the longitudinal direction, backward wave propagation is observed. Fig. 5 shows the simulation results of propagation in z direction with $\Delta t = 0.5(\Delta z)c^{-1}$, 2800-time steps, 900 longitudinal points, and same source used as in the radial simulation. Simple absorbing boundary conditions are applied. The results demonstrate backward wave propagation understood from the negative power flux. Backward energy flow is observed it the bright regions of the figure.

In backward propagation, the electric and magnetic fields propagate opposite to energy flow direction as in the DNG media, the phase velocity is antiparallel to the Poynting vector [4, 12].

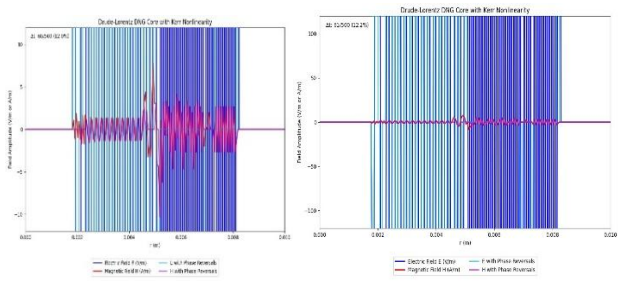

a b

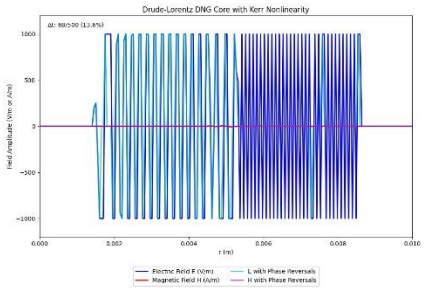

c

Fig. 4 – Snapshots from the 1D simulation of the wave propagation: a) nonlinear dispersive material at $t = 60\Delta t$, b) nonlinear dispersive material at $t = 61\Delta t$, 10 times amplified view, c) nonlinear dispersive material at $t = 68\Delta t$, 100 times amplified view

Interpreting Fig. 3 and Fig. 4 makes us understand that there is smooth propagation in the linear case whereas the nonlinear case shows distorted and confined profiles due to Kerr self-focusing. Directions of radial mode propagations are towards the boundary. As the simulation gives animations as outputs snapshots at different time steps are given. Animations or their python codes may also be used additionally in case supplementary materials are necessary. Different colours in Fig. 4 or the movement opposite to r direction in the animations show phase reversals of the propagation, a substantive result for DNG materials due to reversing phase velocities, distortion due to dispersion or nonlinearity effects like self-reflection or self-scattering. The novel graphical demonstrations in this paper are new as to our knowledge.

The electric field profile shows the actual behaviour of the propagation. As backward waves are fundamentally related to the Poynting vector, and as E and H can have unusual phase relationships in DNG media, both are considered, but longitudinal electric field E_z and the pointing vector S are used to demonstrate backward waves. Fig. 5 shows the backward wave behaviour.

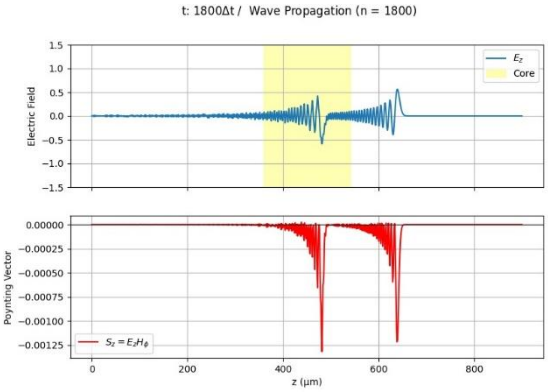

Fig. 5 – 1D simulation of the longitudinal wave propagation in nonlinear dispersive material core; E_z and S at $t = 1800\Delta t$

From the 2D simulation results, we can observe mode transformation with increasing intensity starting from source location and see confinement along the waveguide axis. As a result of the Kerr effect, E_z field forms self-focusing waves [15, 22]. a finding consistent with potential mode shaping in DNG materials. Fig. 6 and Fig. 7 show respectively the field patterns for linear nondispersive and nonlinear dispersive DNG Metamaterials. The simulation results of Fig. 7d and 7e are obtained using $R = 5.0$ mm, $L = z_{\max} = 20$ cm, $\Delta r = R/80$, $\Delta z = L/160$ and the same source.

We see from the results that in linear core, the wave symmetrically develops from the source location, no self-focusing is observed and the field pattern remains smooth and uniform, a demonstration of constant refractive index.

When the core material is nonlinear, however, self-focusing is visible the beam narrows radially as it propagates, a consequence of the Kerr nonlinearity causing the beam to confine itself. We can say that nonlinear DNG waveguides can support self-trapped modes. This can be used for tunable optical guiding and switching applications.

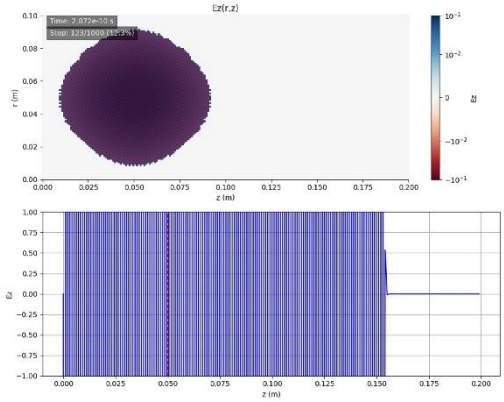

Fig. 6 - 2D simulation of the wave propagation in linear nondispersive material at $t = 123\Delta t$

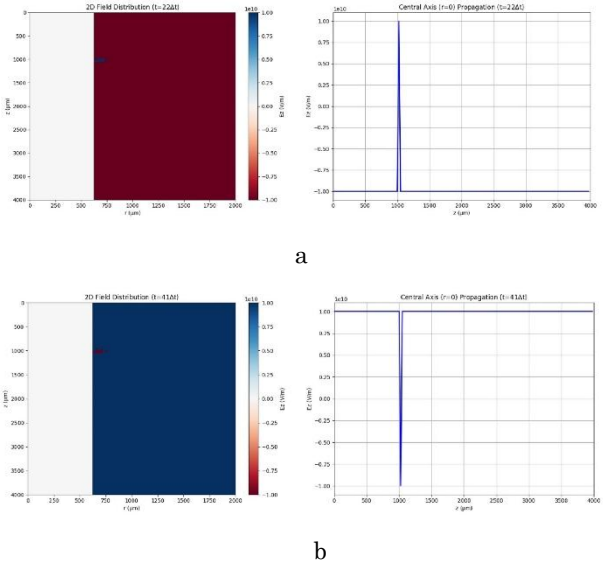

a b

Fig. 7 - 2D simulation of the wave propagation in nonlinear dispersive material a) at t=22Δt, b) at t=41Δt

In our 3D linear nondispersive example, the radial and azimuthal magnetic fields and the longitudinal electric field variations are determining the propagation in the waveguide. Fig. 7 shows snapshot of the field at two different time steps at a fixed φ value.

As simulation example, a case with circular symmetry and following assumptions is analysed and simulated:

Taking only E_z component for simplicity in the spatial 3D FDTD, for TM configuration, with parameters as $\omega_p = 2p10^{12}$ s^{-1}, $\omega_0 = p10^{12}$ s^{-1}, $\gamma_e = \gamma_m = 2p10^{12}$ s^{-1}, $\chi^{(3)} = 10^{-20}$ m^{2}V^{-2}, $\Delta r = \Delta z = 1$ mm, $N_t = 1000$ steps, Gaussian beam source excitation as in Eq. (49) in the middle of radial and azimuthal directions, and on 1/4th of the longitudinal one, $\Delta t \leq 0.99c^{-1}((\Delta r)^{-2} + (r\Delta\varphi)^{-2} + (\Delta z)^{-2})^{-1/2}$ also known as CFL condition is valid for time step, and having PEC cladding. This model avoids $r = 0$ by shifting to $r = \Delta r$ with *grid* $(r, \varphi, z) = (20, 36, 60)$.

Simulation results of case one and case two of nonlinear dispersive waveguide are given in Fig. 8 showing fixed plane slices, Fig. 9 showing full 3D view of field profile in the cylindrical waveguide visualized in Cartesian coordinates. The 3D plots are in scatter diagrammatic view as the grid counts used are few in numbers not to make the calculation too expensive and is more suitable for scatter view instead of a continuous interpolated visualization. It is observed in full 3D simulations that hybrid guided modes involving azimuthal dependence also exist.

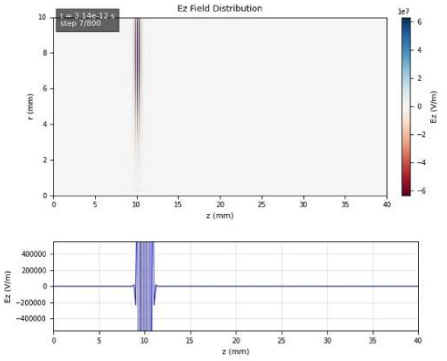

Fig. 8 - Snapshot of the fixed plane slice from the 3D simulation of the wave propagation in linear nondispersive material at $t = 7\Delta t$

The result in Fig. 8 shows a slice revealing the variation of the longitudinal field E_z in radial and longitudinal directions. It has a symmetric pattern without distortion as expected for linear nondispersive core medium.

In 3D nonlinear dispersive case as shown in Fig. 9, we observe first two TM modes and see the longitudinal electric field profile. Normally, in 3D full wave simulation hybrid modes with azimuthal dependence are expected to be the outcomes of the modelling. In our simulation example, we have assumed the axisymmetric case without azimuthal dependence, and this ϕ symmetry causes visual overlap of lobes so that the animations or the snapshots at same time steps seem very similar for both TM modes. Fig. 9 shows TM_{01} and TM_{02} modes electric field profile at same time steps.

TM_{01} has no zero in the core, no radial node, maximum at central axis and vanishing at the PEC cladding boundary. So, it must have low cutoff frequency, high group velocity being lesser dispersive and with very low nonlinearity effects, being respectively stable.

TM_{02}, on the other hand, has a zero inside core. It has opposite signed inner and outer lobes, having high cutoff frequency and low group velocity, shows strong nonlinearity effects being very dispersive, and oscillations are observed. It has one radial node, has a complex electromagnetic structure with rapid magnitude changes, maximum at radial centre, zero at axis, vanishing at PEC boundary, reforming forward waves and enabling also backward waves. For backward waves the wave number and Poynting vector signs are checked. Fig. 10 gives the backward wave diagnostics for the two modes and the radial field profile of normalized E_z for TM_{01} and TM_{02}. Normalization is done using

$$E_{zn}(r) = \frac{E_z(r)}{\max|E_z(r)|} \tag{57}$$

satisfying $max|E_z(r)| = 1$ within $0 < r < R$. Analytic modes of the Bessel functions are used for normalization for the radial profiles only whereas in the FDTD simulations, $E_z(r,z,t)$ is taken without explicit normalization. For the TM modes, E_z field profile is proportional to the Bessel function of the corresponding order. In this simulation example, the first and second zeros of the Bessel function of zero order are the eigenvalues used for solution.

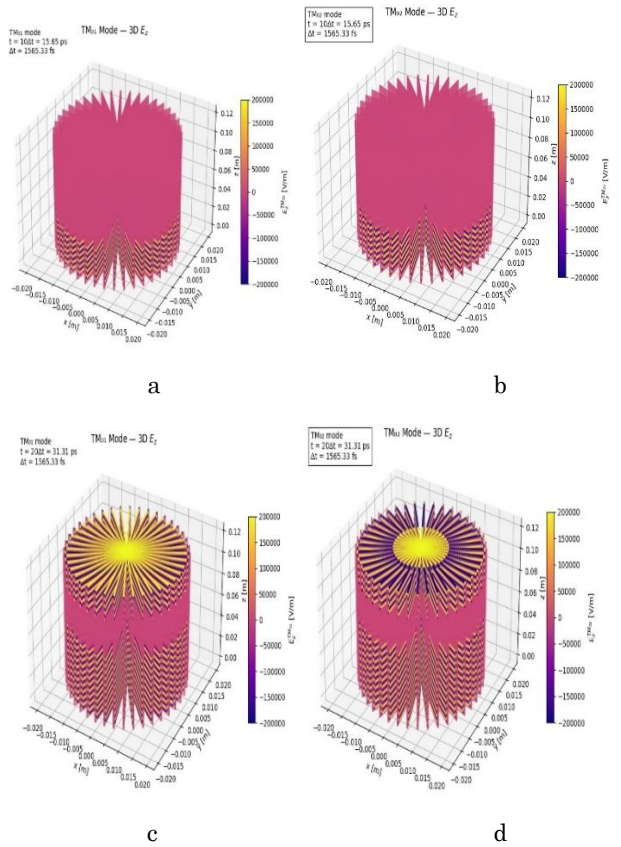

Fig. 9 - Snapshots from the 3D simulation of 3D nonlinear dispersive cylindrical wave propagation: E_z field profile for a) TM_{01} mode at $t = 10\Delta t$, b) TM_{02} mode at $t = 10\Delta t$, c) TM_{01} mode at $t = 20\Delta t$, d) TM_{02} mode at $t = 20\Delta t$

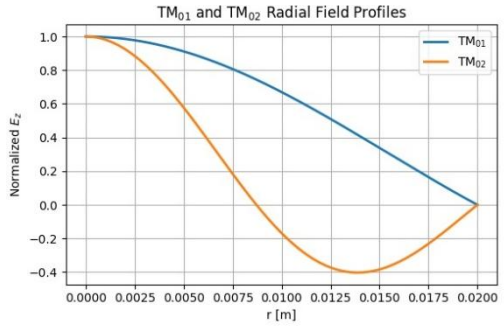

a

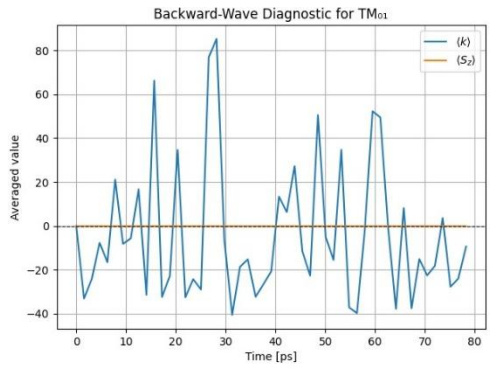

b

Fig. 10 - a) Normalized E_z radial field profiles for TM_{01} and TM_{02}, b) Backward-wave diagnostic for TM_{01}

The simulation of 3D nonlinear propagation suggests actually to solve the full set of six Maxwell equations given in Section 2, but for simplicity and on purpose of also reducing computation costs, a simplified TM/TE formulation used in that specific case. A full component 3D simulation will be incorporated in a future work.

Results are displayed in Cartesian coordinates but modelled so that it represents cylindrical coordinates. As for TM modes, the field component E_z is dominant, it is both more important and easier than the H_ϕ to use in visualization and analysis of the metamaterial properties.

5. CONCLUSIONS

We investigated in this study the propagation of electromagnetic waves in cylindrical waveguides with Kerr-type nonlinear DNG metamaterial cores using the ADE-FDTD method, trying to be comprehensive in the presentation of ADE-FDTD. The simulations carried out include 1D, 2D, and 3D configurations, presenting wave propagation characteristics special to nonlinear and dispersive media. Main findings are backward wave propagation, nonlinear modes, and complex 3D fields. In all three cases, propagation in linear nondispersive waveguides is also checked and compared to the nonlinear dispersive ones.

In 1D simulations, we can observe the backward wave propagation clearly, a distinguishing property of DNG metamaterials. There, phase velocity opposes the energy flow direction. The influence of Kerr nonlinearity is obvious in this phenomenon with its intensity-dependent characteristics resulting in inhomogeneous filed profiles. Phase reversal of fields in radial direction is detected.

Regarding the 2D simulations, the Kerr effect led to self-focusing of the electric field, and nonlinear modes were formed as a result. With dependence on intensities, and showing confinement along longitudinal axis, they demonstrate potential for tunability of such waveguides.

Finally, the 3D simulations normally expected to show hybrid modes with dependence on azimuthal coordinate and exhibiting the interaction of features cylindrical geometry and nonlinear dispersive properties core, did not show this results in the paper as the simulation example was assuming circular symmetry to avoid azimuthal dependence but losing a 3D full wave analysis. So, a scattering wave behaviour with some limitations is analysed and novel finding such as non-complete but physically rigorous outcomes are observed.

The results show that even neglecting small effects, low order contributions or low order slicing causes significant profile changes, emphasizing the need for careful treatment regarding singularities. The geometric meaning of visualizing cylindrical propagation in a Cartesian frame and visualizing cylindrical propagation in a cylindrical frame highlights the 3D electromagnetic mode dynamics.

The study underscores the robust usage of ADE-FDTD method in handling with dispersive nonlinear cylindrical metamaterial waveguides due to the ability of the method to solve Maxwell's equations and ADE concurrently. It demonstrates the presence of unusual profiles of modes in such waveguides, highlighting meanwhile the application potential of them in tuneable optical device areas or photonic systems. The novel application in the study is the use of ADE-FDTD method for analysis of a cylindrical waveguide with a core consisting completely of DNG metamaterial. Experimental validation of these theoretical findings is expected to be achieved in future research. Extension of nonlinear models, and their integration into photonic circuits are other promising areas for further research. This study contributes to comprehension of wave propagation in DNG media with the previously mentioned properties and is expected to encourage and facilitate further exploration of nonlinear dispersive cylindrical metamaterial DNG waveguide structures.

APPENDIX

Explicit Formulae of C1 to C10, G1 to G10, F1 to F9 and A1 to A6

$$C1^n_{r,z}[i,k,\Delta z,\Delta r] = C11^n_{r,z}[i,k,\Delta z] - C12^n_{r,z}[i,k,\Delta r] \quad \text{(AP.1)}$$

$$C11^n_{r,z}[i,k,\Delta z] = \frac{E^n_r[i,k+1] - E^n_r[i,k]}{\Delta z}, \quad \text{(AP.2)}$$

$$C12^n_{r,z}[i,k,\Delta r] = \frac{E^n_z[i+1/2,k] - E^n_z[i-1/2,k]}{\Delta r} \quad \text{(AP.3)}$$

$$C2^n_\varphi[i,k] = M^{n+1/2}_\varphi[i,k] - M^{n-1/2}_\varphi[i,k] \quad \text{(AP.4)}$$

$$C3_{\varphi}^{n}[i,k,\Delta z]=\frac{E_{\varphi}^{n}[i+1/2,k+1]-E_{\varphi}^{n}[i+1/2,k]}{\Delta z} \quad \text{(AP.5)}$$

$$C4_{r}^{n}[i,k]=M_{r}^{n+1/2}[i,k]-M_{r}^{n-1/2}[i,k] \quad \text{(AP.6)}$$

$$C5_{\varphi,r}^{n}[i,k,\Delta r]=C51_{\varphi,r}^{n}[i,k,\Delta r]-C52_{\varphi,r}^{n}[i,k,\Delta r] \quad \text{(AP.7)}$$

$$C51_{\varphi,r}^{n}[i,k,\Delta r]=\frac{E_{\varphi}^{n}[i+1/2,k+1/2]-E_{\varphi}^{n}[i-1/2,k+1/2]}{\Delta r}, \quad \text{(AP.8)}$$

$$C52_{\varphi,r}^{n}[i,k,\Delta r]=\frac{E_{\varphi}^{n}[i+1/2,k+1/2]+E_{\varphi}^{n}[i-1/2,k+1/2]}{2(i)\Delta r} \quad \text{(AP.9)}$$

$$C6_{z}^{n}[i,k]=M_{z}^{n+1/2}[i,k]-M_{z}^{n-1/2}[i,k] \quad \text{(AP.10)}$$

$$C7_{\varphi}^{n}[i,k,\Delta z]=-\frac{H_{\varphi}^{n+1/2}[i,k+1]-H_{\varphi}^{n+1/2}[i,k]}{\Delta z} \quad \text{(AP.11)}$$

$$C8_{r}^{n}[i,k]=P_{NL,r}^{n+1}[i,k]-P_{NL,r}^{n}[i,k]+P_{L,r}^{n+1}[i,k]-P_{L,r}^{n}[i,k] \quad \text{(AP.12)}$$

$$C9_{r,z}^{n}[i,k,\Delta z,\Delta r]=C91_{r,z}^{n}[i,k,\Delta z]-C92_{r,z}^{n}[i,k,\Delta r] \quad \text{(AP.13)}$$

$$C91_{r,z}^{n}[i,k,\Delta z]=-\frac{H_{r}^{n+1/2}[i+1/2,k+1/2]-H_{r}^{n+1/2}[i+1/2,k-1/2]}{\Delta z} \quad \text{(AP.14)}$$

$$C92_{r,z}^{n}[i,k,\Delta r]=\frac{H_{z}^{n+1/2}[i+1,k]-H_{r}^{n+1/2}[i,k]}{\Delta r} \quad \text{(AP.15)}$$

$$C10_{\varphi}^{n}[i,k]=P_{NL,\varphi}^{n+1}[i,k]-P_{NL,\varphi}^{n}[i,k]+P_{L,\varphi}^{n+1}[i,k]-P_{L,\varphi}^{n}[i,k] \quad \text{(AP.16)}$$

$$G1_{\varphi}^{n}[i,k,\Delta r]=\frac{1}{(i+1/2)}\frac{(i+1)H_{\varphi}^{n+1/2}[i+1,k]-(i)H_{\varphi}^{n+1/2}[i,k]}{\Delta r} \quad \text{(AP.17)}$$

$$G2_{z}^{n}[i,k]=P_{NL,z}^{n+1}[i,k]-P_{NL,z}^{n}[i,k]+P_{L,z}^{n+1}[i,k]-P_{L,z}^{n}[i,k] \quad \text{(AP.18)}$$

$$G3_{\varphi}^{n}[i,k]=r[i+1/2]E_{\varphi}^{n}[i+1/2,k]-r[i-1/2]E_{\varphi}^{n}[i-1/2,k] \quad \text{(AP.19)}$$

$$G4_{z}^{n}[i,k]=H_{z}^{n+1/2}[i+1,k]-H_{z}^{n+1/2}[i,k] \quad \text{(AP.20)}$$

$$G5_{z}^{n}[i,k]=H_{z}^{n+1/2}[i,k+1]-H_{z}^{n+1/2}[i,k] \quad \text{(AP.21)}$$

$$G6_{z,\varphi}^{n}[i]=E_{z}[i+1]-E_{z}[i]-(M_{\varphi}[i+1]-M_{\varphi}[i]) \quad \text{(AP.22)}$$

$$G7_{\varphi,z}^{n}[i,\Delta r]=\frac{H_{\varphi}[i]-H_{\varphi}[i-1]}{\Delta r}-\frac{P_{z}[i]-P_{z}[i-1]}{\Delta r}-3\chi^{(3)}E_{z}^{2}[i]E_{z}[i] \quad \text{(AP.23)}$$

$$G8_{\varphi}^{n}[i]=\omega_{m}^{2}H_{\varphi}[i]-\gamma_{m}M_{\varphi}[i]-\omega_{0}^{2}M_{\varphi}[i-1] \quad \text{(AP.24)}$$

$$G9_{z}^{n}[i,k,\Delta r]=\frac{E_{z}^{n}[i+1,k]-E_{z}^{n}[i,k]}{\Delta r} \quad \text{(AP.25)}$$

$$G10_{z}^{n}[i,k,\Delta z]=\frac{E_{z}^{n}[i,k+1]-E_{z}^{n}[i,k]}{\Delta z} \quad \text{(AP.26)}$$

$$F1_{r,z,\varphi}^{n}[i,k,\Delta r,\Delta z]=F11_{r,\varphi}^{n}[i,k,\Delta r]-F12_{r,z}^{n}[i,k,\Delta z], \quad \text{(AP.27)}$$

$$F11_{r,z}^{n}[i,k,\Delta r]=\frac{1}{r[i]}\frac{r[i+1/2]H_{\varphi}^{n+1/2}[i+1/2,k]-r[i-1/2]H_{\varphi}^{n+1/2}[i-1/2,k]}{\Delta r} \quad \text{(AP.28)}$$

$$F12_{r,z}^{n}[i,k,\Delta z]=\frac{H_{r}^{n+1/2}[i,k+1/2]-H_{r}^{n+1/2}[i,k+1/2]}{\Delta z} \quad \text{(AP.29)}$$

$$F2_{r,z}^{n}[i,k,\Delta r,\Delta z]=F21_{r,z}^{n}[i,k,\Delta r]-F22_{r,z}^{n}[i,k,\Delta z], \quad \text{(AP.30)}$$

$$F21_{r,z}^{n}[i,k,\Delta r]=\frac{E_{z}^{n}[i,k]-E_{z}^{n}[i-1,k]}{\Delta r}, \quad \text{(AP.31)}$$

$$F22_{r,z}^{n}[i,k,\Delta z]=\frac{E_{r}^{n}[i,k+1]-E_{r}^{n}[i,k]}{\Delta z} \quad \text{(AP.32)}$$

$$F3_{\varphi}^{n}[i,k]=\frac{M_{\varphi}^{n}[i,k+1]-M_{\varphi}^{n-1}[i,k]}{\Delta t} \quad \text{(AP.33)}$$

$$F4_{r,\varphi}^{n}[i,k,\Delta r]=\frac{r[i+1/2]H_{\varphi}^{n+1/2}[i,k]-r[i-1/2]H_{\varphi}^{n+1/2}[i-1,k]}{r[i]\Delta r} \quad \text{(AP.34)}$$

$$F5_{r}^{n}[i,k]=F51_{r}^{n}[i,k]+F52_{r}^{n}[i,k], \quad \text{(AP.35)}$$

$$F51_{r}^{n}[i,k]=\frac{P_{NL,r}^{n+1}[i,k]-P_{NL,r}^{n-1}[i,k]}{\Delta t}, \quad \text{(AP.36)}$$

$$F52_{r}^{n}[i,k]=\frac{P_{L,r}^{n+1}[i,k]-P_{L,r}^{n-1}[i,k]}{\Delta t} \quad \text{(AP.37)}$$

$$F6_{r,\varphi}^{n}[i,k,\Delta r]=\frac{H_{\varphi}^{n+1/2}[i,k]-H_{\varphi}^{n+1/2}[i-1,k]}{\Delta r} \quad \text{(AP.38)}$$

$$F7_{r}^{n}[i,k]=F71_{r}^{n}[i,k]+F72_{r}^{n}[i,k], \quad \text{(AP.39)}$$

$$F71_{r}^{n}[i,k]=\frac{P_{NL,z}^{n+1}[i,k]-P_{NL,z}^{n}[i,k]}{\Delta t}, \quad \text{(AP.40)}$$

$$F72_{r}^{n}[i,k]=\frac{P_{L,z}^{n+1}[i,k]-P_{L,z}^{n}[i,k]}{\Delta t} \quad \text{(AP.41)}$$

$$F8_{z}^{n}[i,k,\Delta r]=\frac{E_{z}^{n}[i+1,k]-E_{z}^{n}[i,k]}{\Delta r} \quad \text{(AP.42)}$$

$$F9_{z}^{n}[i,k,\Delta z]=\frac{E_{z}^{n}[i,k+1]-E_{z}^{n}[i,k]}{\Delta z} \quad \text{(AP.43)}$$

$$A1_{z,r,\varphi}^{n}[i,k,\Delta z,\Delta r]=A11_{r,\varphi}^{n}[i,k,\Delta r]-A12_{z,\varphi}^{n}[i,k,\Delta z], \quad \text{(AP.44)}$$

$$A11_{r,\varphi}^{n}[i,k,\Delta r]=\frac{r[i+1/2]H_{\varphi}^{n+1/2}[i+1/2,k]-r[i-1/2]H_{\varphi}^{n+1/2}[i-1/2,k]}{r[i]\Delta z}, \quad \text{(AP.45)}$$

$$A12_{z,\varphi}^{n}[i,k,\Delta z]=\frac{H_{\varphi}^{n+1/2}[i,k+1/2]-H_{\varphi}^{n+1/2}[i,k-1/2]}{\Delta z} \quad \text{(AP.46)}$$

$$A2_{r,z}^{n}[i,k,\Delta r]=\frac{E_{z}^{n+1}[i+1,k]-E_{z}^{n+1}[i,k]}{\Delta r} \quad \text{(AP.47)}$$

$$A3_{\varphi}^{n}[i,k]=\frac{M_{\varphi}^{n+1}[i+1/2,k]-M_{\varphi}^{n}[i+1/2,k]}{\Delta t} \quad \text{(AP.48)}$$

$$A4_{r,\varphi}^{n}[i,k,\Delta r]=\frac{H_{\varphi}^{n}[i+1/2,k]-H_{\varphi}^{n}[i-1/2,k]}{\Delta r} \quad \text{(AP.49)}$$

$$A5_{z}^{n}[i,k]=\frac{P_{z}^{n+1}[i,k]-P_{z}^{n}[i,k]}{\Delta t} \quad \text{(AP.50)}$$

$$A6_{r,\varphi,z}^{n}[i,k]=\frac{H_{\varphi}^{n}[i,k]}{r[i]}-P_{NL,z}^{n}[i,k] \quad \text{(AP.51)}$$

REFERENCES

1. V.G. Veselago, *Sov. Phys. Usp.* **10** 509 (1968) http://dx.doi.org/10.1070/PU1968v010n04ABEH003699.
2. R.A. Shelby, D.R. Smith, S. Schultz, *Science* **292** 77 (2001) https://doi.org/10.1126/science.1058847.
3. H. Zhang, Y. Zhou, *2012 Int. Con. on Microw. Millimetre Wave Technology (ICMMT)* (Shenzhen: 2012) https://doi.org/10.1109/ICMMT.2012.6230140
4. J G. Pollock, A.K. Iyer, *IEEE Trans. Microw. Theory Tech* **61** 3169 (2013) https://doi.org/10.1109/TMTT.2013.2274780.
5. L. Wang, S-J. Lai, Z-Y. Duan, *2010 Int. Conf. Microw. Millimeter Wave Technol.* (Chengdu: 2010). https://doi.org/10.1109/ICMMT.2010.5525278.
6. Q. Zhang, T. Jiang, Y. Feng, *J. Phys. D: Appl. Phys.* **44** 475103 (2011) https://doi.org/10.1088/0022-3727/44/47/47510.
7. H.V. Shojaa, A. Araba, M.S. Farb, *Int. J. Opt. Photon. (IJOP)* **9**, 3 (2015).
8. Z. Fan, J. Sun, Y. Cao, Z. Song, P. Wu, Y. Shi, *AIP Adv.* **9** 085033 (2019) https://doi.org/10.1063/1.5099078.
9. S. Lufa, W. Zihua, *Optoelectron. Lett.* **3** 257 (2007) https://doi.org/10.1007/s11801-007-6185-1.
10. B. Ghosh, A.B. Kakade, *Electromagnetics* **32**, 465 (2012) https://doi.org/10.1080/02726343.2012.726913.
11. A.V. Novitsky, L.M. Barkovsky, *J. Opt. A: Pure Appl. Op.* **7** S51 (2005) http://dx.doi.org/10.1088/1464-4258/7/2/007.
12. P. Porfyrakis, N.L. Tsitsas, *Microelectron. Eng.* **216** 111028 (2019) https://doi.org/10.1016/j.mee.2019.111028.
13. K.S. Yee, *IEEE Trans. Antennas Propag.Ap-14* **3**, 302 (1966).
14. K. Kawano, T. Kitoh, *Introduction to Optical Waveguide Analysis* (New York: John Wiley & Sons: 2001).
15. K. Okamato, *Fundamentals of Optical Waveguides* (London: Academic Press: 2nd ed: 2006).
16. N. Dib, T. Weller, M. Scardelletti, *1998 IEEE MTT-S International Microwave Symposium Digest (Cat. No.98CH36192)* (Baltimore: 1998) https://doi.org/10.1109/MWSYM.1998.705142.
17. C. Goswami, S. Mukherjee, S. Karmakar, M. Pal, R. Ghatak, *J Electromagn Anal Appl.* **6** 106 (2014). https://doi.org/10.4236/jemaa.2014.65010.
18. Y. Takayama, W. Klaus, *IEEE Microw. Wirel. Compon. Lett.* **12** 102 (2002) https://doi.org/10.1109/7260.989865.
19. L. Pauk, Z. Skvor, *EUROCON'2001 Int. Conf. on Trends in Communications Technical Program, (Proc. Cat.No.01EX439)* (Bratislava: 2001) https://doi.org/10.1109/EURCON.2001.938123.
20. N. Dib, T. Weller, *Int. J. Electron.* **87** 1065 (2000) https://doi.org/10.1080/002072100413000.
21. M.A. Alsunaidi, A. Al-Jabr, *IEEE Photonic. Tech. L.* **21** 817 (2009) https://doi.org/10.1109/LPT.2009.2018638.
22. G-Y. Liu, W-J. Chen, J. Quan, *IEEE Microw. Wirel. Co.* **32** 1391 (2022) https://doi.org/10.1109/LMWC.2022.3184044.
23. Z. Kancleris, *IEEE T. Anten. Propag.* **56** 610 (2008) https://doi.org/10.1109/TAP.2007.915478.
24. B. Chen, *MATEC Web of Conferences* **309** 01002 (2020) https://doi.org/10.1051/matecconf/202030901002.
25. A. Munir, B.T. Ranum, *1st Int. Conf. on Wireless and Telematics* (Manado: 2015) https://doi.org/10.1109/ICWT.2015.7449251.

Моделювання поширення хвиль у циліндричному хвилеводі з нелінійного метаматеріалу типу Керра за допомогою методу скінченних різниць у часовій області допоміжних диференціальних рівнянь

A. Yalçınkaya[1], A. Çetin[2]

[1] *Eskişehir Osmangazi University, Graduate School of Natural and Applied Sciences, Eskişehir, Turkiye*
[2] *Eskişehir Osmangazi University, Faculty of Science, Meşelik Kampüsü, Eskişehir, Turkiye*

У цій роботі розглядається поширення електромагнітних хвиль та формування мод у циліндричному хвилеводі з подвійним негативним метаматеріальним осердям, що має нелінійність типу Керра. Досліджується поширення в одновимірній, двовимірній та тривимірній конфігураціях, а також виділяється взаємодія властивостей, що стосуються дисперсії, нелінійності та циліндричної структури, з акцентом на її вплив на поведінку мод. Дискретизовані рівняння, представлені в статті, відрізняються від усіх рівнянь, представлених у попередніх дослідженнях на основі скінченно-різницевих часових областей та відповідній літературі. Нове застосування, використане в цій роботі для дослідження динаміки хвиль у циліндричному осерді з повністю подвійно негативного метаматеріалу, показало нові результати. Спостерігаються поширення зворотної хвилі та самофокусуючі нелінійні моди через подвійні негативні властивості та ефект Керра, як і очікувалося. Очікується, що результати сприятимуть дослідженням нелінійної волоконної оптики та привернуть увагу до метаматеріалів та того, як спостерігається вплив втрат у метаматеріальних хвилеводах.

Ключові слова: Метаматеріал, Циліндричний хвилевід, Нелінійність Керра, Часова область скінченних різниць, Допоміжне диференціальне рівняння.